

Adaptive Pore Opening to Form Tailored Adsorption Sites in a Cooperatively Flexible Framework Enables Record Inverse Propane/Propylene Separation

Ryan A. Klein,[▽] Lukas W. Bingel,[▽] Arijit Halder, Marcus Carter, Benjamin A. Trump, Eric D. Bloch, Wei Zhou, Krista S. Walton, Craig M. Brown, and C. Michael McGuirk*



Cite This: *J. Am. Chem. Soc.* 2023, 145, 21955–21965



Read Online

ACCESS |



Metrics & More

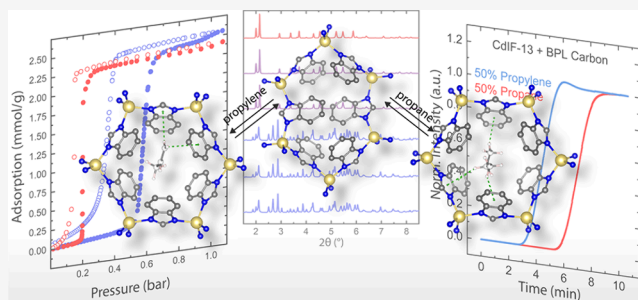


Article Recommendations



Supporting Information

ABSTRACT: A proposed low-energy alternative to the separation of alkanes from alkenes by energy-intensive cryogenic distillation is separation by porous adsorbents. Unfortunately, most adsorbents preferentially take up the desired, high-value major component alkene, requiring frequent regeneration. Adsorbents with inverse selectivity for the minor component alkane would enable the direct production of purified, reagent-grade alkene, greatly reducing global energy consumption. However, such materials are exceedingly rare, especially for propane/propylene separation. Here, we report that through adaptive and spontaneous pore size and shape adaptation to optimize an ensemble of weak noncovalent interactions, the structurally responsive metal–organic framework CdIF-13 (*sod*-Cd(benzimidazolate)₂) exhibits inverse selectivity for propane over propylene with record-setting separation performance under industrially relevant temperature, pressure, and mixture conditions. Powder synchrotron X-ray diffraction measurements combined with first-principles calculations yield atomic-scale insight and reveal the induced fit mechanism of adsorbate-specific pore adaptation and ensemble interactions between ligands and adsorbates. Dynamic column breakthrough measurements confirm that CdIF-13 displays selectivity under mixed-component conditions of varying ratios, with a record measured selectivity factor of $\alpha \approx 3$ at 95:5 propylene:propane at 298 K and 1 bar. When sequenced with a low-cost rigid adsorbent, we demonstrated the direct purification of propylene under ambient conditions. This combined atomic-level structural characterization and performance testing firmly establishes how cooperatively flexible materials can be capable of unprecedented separation factors.



INTRODUCTION

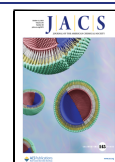
Ethylene (C₂H₄) and propylene (C₃H₆) are arguably the most important chemical feedstocks today.^{1–5} Annual global production reached 170 million tons of ethylene and 120 million tons of propylene in 2016¹ and is expected to increase to 220 million tons of ethylene and 130 million tons of propylene this year.⁶ Unfortunately, the production of these alkenes by high-temperature steam-cracking of petrochemical feeds also generates significant alkane impurities, requiring purification.³ However, because of the structural and physicochemical similarities of ethylene with ethane and propylene with propane, state-of-the-art purification processes involve exceedingly energy-intensive distillations, requiring large towers with precise control of high pressures and cryogenic temperatures.^{6,7} As such, finding an alternative to cryogenic distillation for alkene/alkane (olefin/paraffin) separation is an outstanding challenge today as it has the potential to greatly reduce global energy consumption and carbon footprint.¹ One potential low-energy alternative is adsorptive separation using porous materials packed as fixed beds,^{8–12} wherein the gaseous mixture is flowed through a

column of the porous material. Selective adsorption of one component then yields a purified stream of the other at the column outlet. Progress for ethylene purification has been made using this approach,^{5,13–20} however, propylene purification lags far behind.

A particular challenge for propylene purification is finding materials that can preferentially adsorb the minor component propane, as propylene is both the major component in industrial mixtures (93–95%)²¹ and the desired product. Typically, the olefin is more strongly adsorbed due to the high-lying π -electrons that can interact with Lewis acidic moieties in the sorbent. Selective adsorption of the minor component propane would directly generate purified propylene down-

Received: June 27, 2023

Published: September 29, 2023



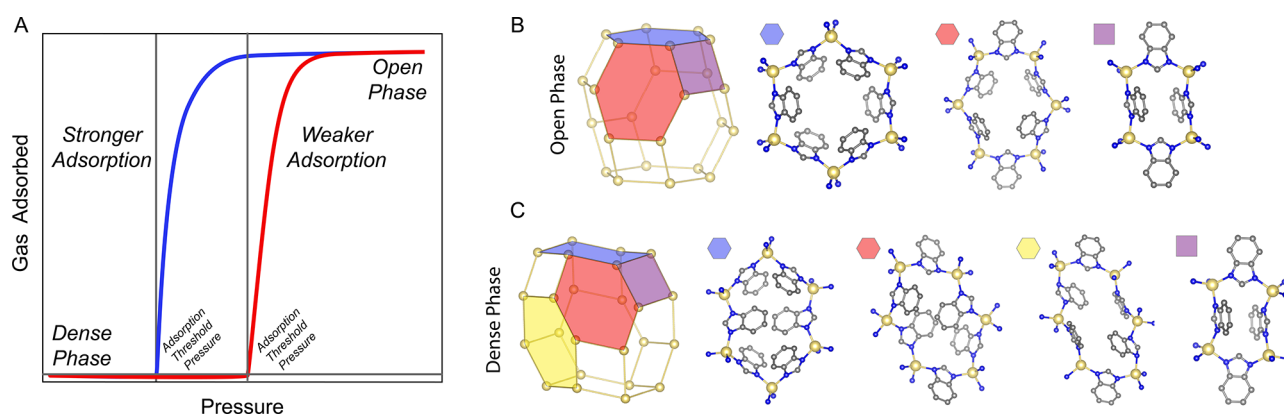


Figure 1. (A) Example gas adsorption isothermal plots for flexible sorbents. The blue plot depicts strong sorption in a flexible material, while the red plot depicts weaker sorption in a flexible material. They are characterized by a prestep regime, corresponding to a dense phase, a step at the phase transition, and a poststep regime corresponding to an open phase. The enthalpy of adsorption of the guest species in part determines the pressure of the step. (B) The open phase of CdIF-13 comprises three distinct rings that combine to give a sodalite-like topology. (C) The dense phase comprises four distinct rings, which combine to give a distorted sodalite-like topology.

stream. Ideally, this would occur at ambient temperatures and pressures, obviating the need for expensive equipment, refrigeration, and pressurization of the gases for purification.⁷ Moreover, adsorbing the minor component reduces the frequency of undesirable, energy-consuming adsorbent regeneration steps. Thus, to achieve improved separations, new materials are needed that effectively invert the common mode of adsorption.

Metal–organic frameworks, permanently porous crystalline networks comprising inorganic nodes linked by polytopic organic ligands, are particularly promising for realizing improved propylene purifications through propane-selective sorption. These materials are highly modular, and the sorption properties can be tuned to an extent by modifying pore size, shape, and electronic surface potential via metal substitution and ligand modifications.^{22–24} However, the *de novo* design and subsequent synthesis of frameworks with the precise pore size, shape, and surface electronics needed to selectively adsorb propane over propylene, particularly under mixed-component conditions, remain exceedingly challenging, stunting this field. While some propane-selective materials have been reported,^{21–37} they display insufficiently low propane/propylene separation factors as derived experimentally from mixed-component breakthrough measurements.³⁸ As such, it appears that a fundamentally alternative approach is needed to improve separation factors at industrially relevant pressure, temperature, and mixture ratio conditions.

While most frameworks are considered rigid, a subset exhibits cooperative, or periodic, structural flexibility. Here, the accessible porosity throughout the entire framework lattice dynamically and reversibly changes in response to small molecule adsorption and desorption. This phase transition manifests as a step in the isothermal plot at a substrate- and temperature-dependent critical pressure (Figure 1A). Substrates that adsorb more strongly to the flexible material induce the step at lower pressures (blue plot, Figure 1A) than do more weakly interacting guest molecules (red plot, Figure 1A).

Compared to rigid frameworks, cooperatively flexible MOFs have been significantly less explored for separations.^{39–42} Nonetheless, the potential of cooperatively flexible frameworks for separations was exemplified by Gücüyener et al. with the seminal report of inverse selectivity for ethane over ethylene and purification of ethylene in the cooperatively flexible

framework ZIF-7 (*sod*-Zn(benzimidazolate)₂) that exhibits step-shaped, or Type V-like, adsorption.⁴³ However, even though this key finding was reported nearly 14 years ago, the precise underlying process enabling inverse selectivity and separation in this and other cooperatively dynamic materials remains very poorly understood at the atomic scale, hindering further informed development of flexible sorbents for critical separation processes.

Indeed, the perception that cooperatively flexible adsorbents cannot be reliably effective in representative mixed-component kinetic separations continues to inhibit the field.^{44–47} The reasoning is that once the pore space becomes more accessible, adsorbates can simply coadsorb in the new space, and the selectivity predicted from single-component measurements is lost. This theorized nonselective coadsorption would be particularly problematic when trying to design materials that preferentially adsorb the minor component, such as with propane/propylene.⁴⁵ We argue that this generalized perception stunting the field is largely due to the lack of atomic-level structural characterization and thus understanding of how cooperatively flexible frameworks adapt to and adsorb different small molecules, leading to selective adsorption that persists during mixed-component separations. For example, with representative ZIF-7, the mechanism enabling selectivity has been investigated using first-principles calculations, but there are no empirical structural studies that support this mechanism. Critically, these calculations were performed before the responsive phase change of ZIF-7 was well understood,⁴⁸ and, as such, are not directly supported by experiments. Thus, overall, there remains significant potential for advancing the atomic-level understanding of adsorption in cooperatively flexible frameworks and how these responsive pore environments can enable rare and record selectivity and separations such as propane/propylene separations.

Previously, we reported a congener of ZIF-7, CdIF-13, (*sod*-Cd(benzimidazolate)₂, (CdC₁₄N₄H₁₀)),^{48,54} which also exhibits cooperative flexibility and step-shaped adsorption, but with nearly 50% greater adsorption capacities, negligible prestep adsorption, and much higher adsorption threshold pressures. For example, whereas ZIF-7 adsorbs propane near 0.008 bar at 298 K,³³ CdIF-13 does so at 0.2 bar, a much-preferred pressure range for ambient temperature adsorptive separation,^{49,50} obviating the need for high temperatures.

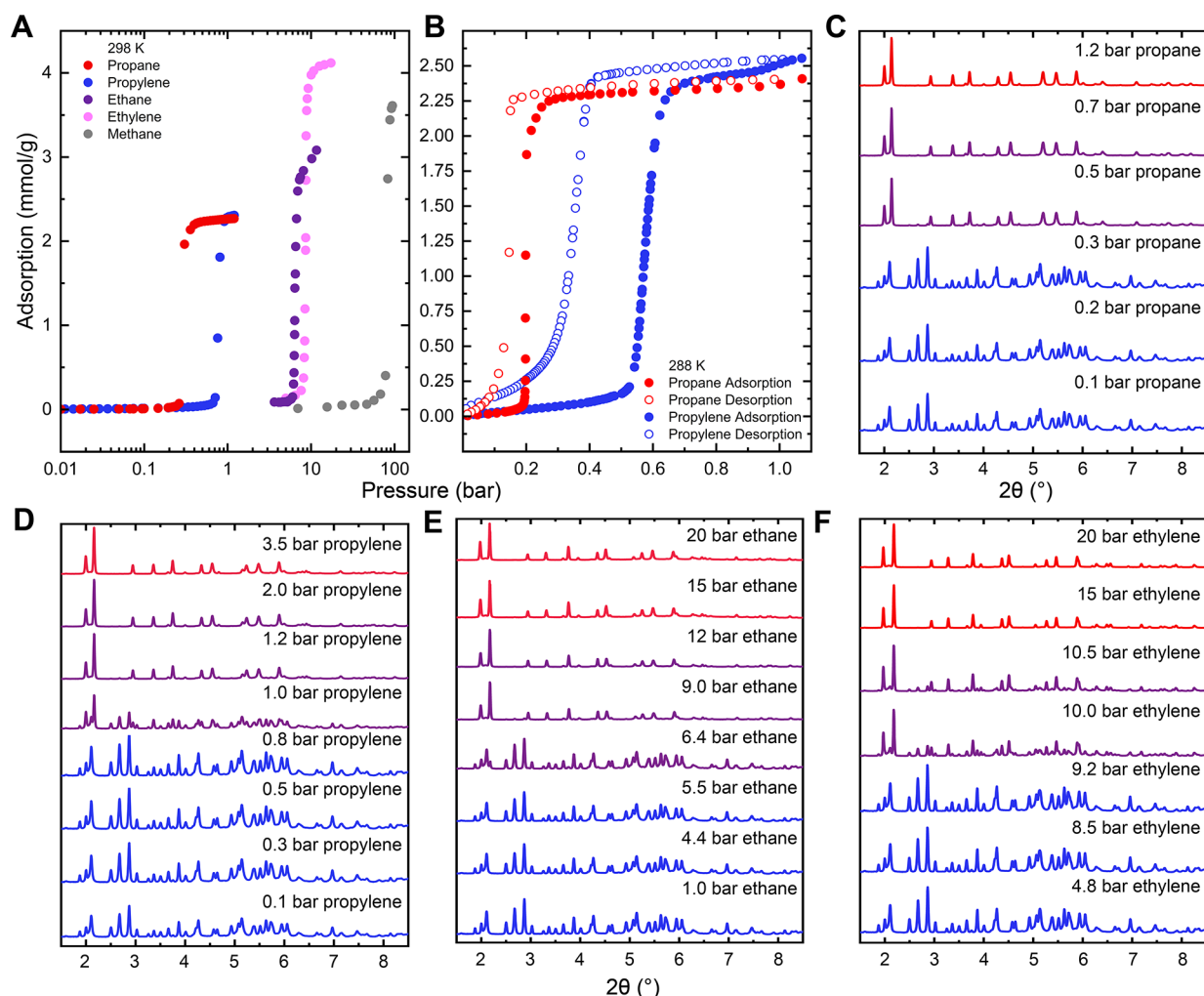


Figure 2. (A) Isothermal adsorption plot for methane, ethane, ethylene, propane, and propylene for CdIF-13. (B) Adsorption and desorption data for propane and propylene, showing modest hysteresis. In situ gas-dosed PSXRD patterns for CdIF-13 dosed with (C) propane, (D) propylene, (E) ethane, and (F) ethylene. Patterns were collected using $\lambda = 0.45191$ Å, 298 K.

Moreover, CdIF-13 retains a high degree of crystallinity through the pressure-induced phase transition, which enabled single crystal X-ray diffraction measurements of the activated phase of CdIF-13 (Figure 1C), which in turn helped us answer the long-standing question of the nature of the dense phase of ZIF-7.⁴⁸ Based on the results of the single-component isothermal adsorption measurements, we hypothesized that a detailed structure–function study of alkane/alkene adsorption in CdIF-13 may yield atomic-scale insight into how selectivity predicted from single-component equilibrium adsorption measurements with cooperatively flexible materials can be conserved under mixed-component separation conditions, leading to effective separations. At the same time, we hypothesized that due to the stepped adsorption threshold pressures, this material may provide highly efficient, direct propylene purification, effectively addressing two outstanding challenges simultaneously: better understanding how cooperatively flexible materials achieve separations and efficiently purifying propylene under ambient conditions.

Here, we report single-component isothermal adsorption measurements for methane, ethane, ethylene, propane, and propylene in CdIF-13 and show that the adsorption step occurs at lower pressures for the alkanes than for the corresponding alkenes, suggesting inverse selectivity. For

propane and propylene, the respective adsorption steps both occur at near-ambient pressures at 298 K, suggesting that this system may display useful separation capabilities at mild pressure–temperature conditions. Furthermore, CdIF-13 exhibits a large separation between the adsorption threshold pressures for propane and propylene, ~ 50 times that of ZIF-7,⁴³ further evidencing that this material may prove useful for propylene purification. We then combined in situ synchrotron powder X-ray diffraction measurements with first-principles calculations to thoroughly investigate the atomic-scale origins of the apparent rare inverse selectivity for adsorbing the paraffins, ethane and propane, over their respective olefins, ethylene and propylene. Namely, adsorbate-dependent pore opening following an induced-fit mechanism produces a tailored adsorption environment for each adsorbate,^{48,51} wherein a high-fidelity ensemble of individually weak C–H $\cdots\pi$ gas–framework interactions produces thermodynamic selectivity for the saturated hydrocarbons. Motivated by the pressure–temperature conditions, suggested inverted selectivity, and large separation of adsorption step thresholds for propane and propylene in CdIF-13, we then conducted dynamic multicomponent breakthrough adsorption measurements. We observed that the inverse selectivity inferred from single-component equilibrium measurements is, in fact,

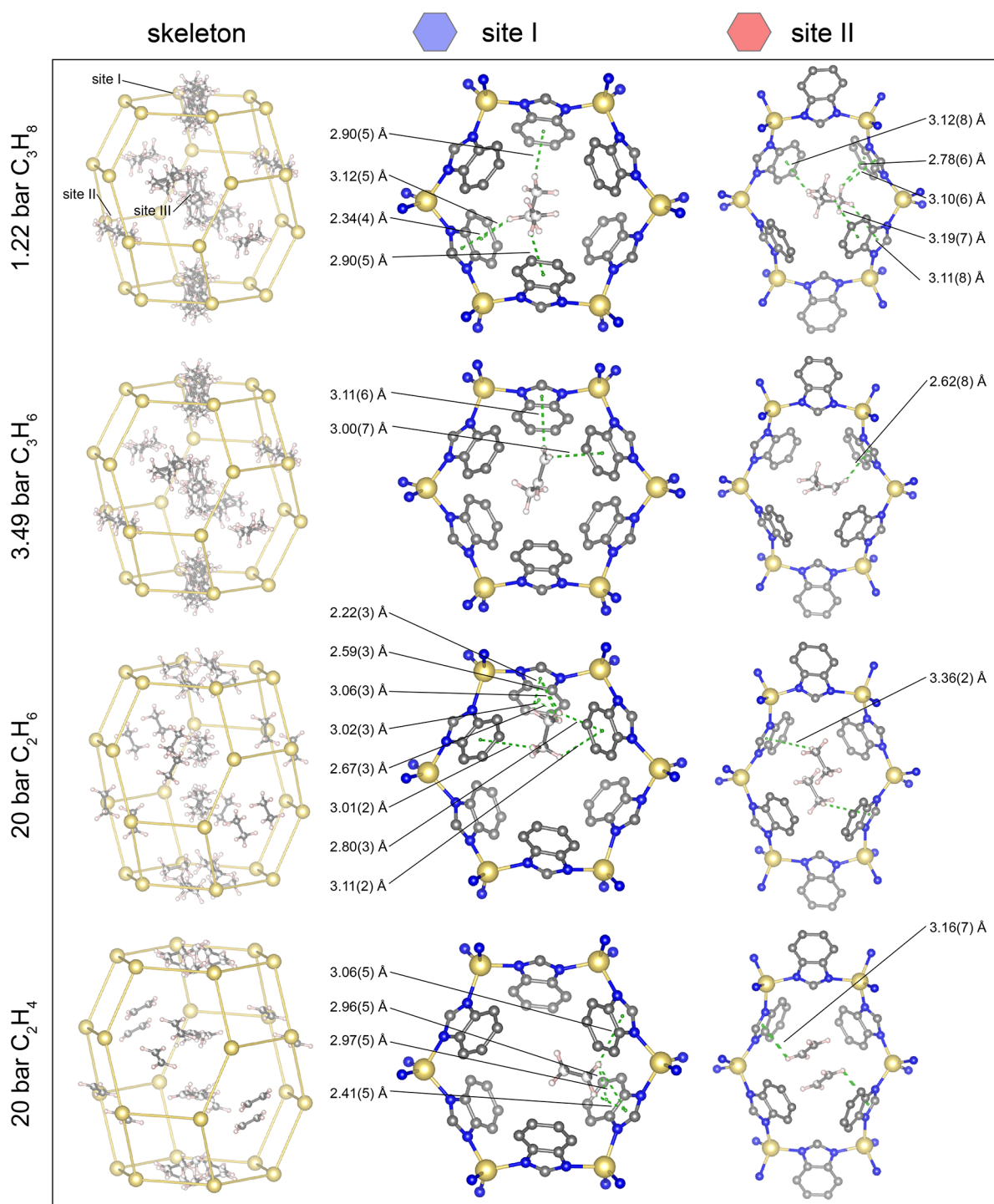


Figure 3. Framework skeletons and three distinct sorption sites are shown for all four gases (left column) at the highest measured pressures, as indicated to the left of the figure. The middle and right columns depict the primary and secondary adsorption sites (sites I and II), respectively, for all four gases. Propane and ethane form more C–H... π interactions, indicated by dashed green lines, with the framework in the primary and secondary adsorption sites than do propylene and ethylene. Yellow, blue, gray, and white spheres depict Cd, N, C, and H atoms, respectively, while framework H atoms are omitted for clarity. Values in parentheses indicate $\pm 1\sigma$ as estimated from adjacent adsorbent–adsorbate C–C estimated standard deviation values. Partial shading denotes the occupancy of the disordered gas molecules.

retained under dynamic mixed-component conditions. Excitingly, CdIF-13 exhibits record high separation factors for propane over propylene, which are maintained across a large range of mixture ratios, including under industrially relevant conditions with propane as the minor component (5%), at room temperature and near-ambient pressure. When used in a recently developed two-column approach with an inexpensive

porous carbon adsorbent, the record selectivity of CdIF-13 enables direct purification of propylene at 1 bar and 298 K.⁵² In summary, we report the direct production of purified propylene under ambient conditions achieved by a cooperatively flexible framework and describe the atomic-scale origins of this record separation.

RESULTS AND DISCUSSION

Single-Component Gas Adsorption. Single-component equilibrium isothermal gas adsorption measurements (Figure 2A,B) indicate that CdIF-13 displays a cooperatively dynamic response to changing pressures of methane, ethane, ethylene, propane, and propylene at ambient temperature, evidenced by step-shaped, or Type V-like, isothermal adsorption–desorption data.⁵³ In the prestep regime, CdIF-13 exists in a dense phase with low accessible porosity and effectively zero gas adsorption for the measured species (Figure 1C). Accordingly, the prestep regimes of the isothermal measurements are effectively flat. At an adsorbate-dependent pressure threshold, CdIF-13 undergoes a phase transition to a more open phase with greater accessible porosity, resulting in steep uptake, or a step, over a narrow pressure window followed by saturation. In the poststep regime, the material exists in a more porous, open phase (Figure 1B).

At 298 K, the step occurs at pressures of ≈ 0.3 , 0.8, 6.4, 8.6, and 80 bar for propane, propylene, ethane, ethylene, and methane, respectively. The lower pressure thresholds for step-shaped adsorption of propane versus propylene and ethane versus ethylene (Figure 2A,B) suggest inverse selectivity for the alkanes over their respective alkenes. Comparatively, ZIF-7 exhibits stepped adsorption thresholds at 298 K of approximately 0.008 and 0.020 bar for propane and propylene, respectively, just a 0.012 bar difference.⁴³ Interestingly, here the poststep regime of the isotherm curves is effectively flat for ethylene, propylene, and propane but sloped for ethane, possibly indicating some slower kinetic component or possible multistep behavior, as observed for CO₂ in CdIF-13,⁵⁴ for this probe gas. We observe higher total adsorption for the C2 gases compared to the C3 gases, likely caused by differences in molecular size.

Probing Structure–Function Relationships. *In Situ Gas-Dosed Powder Diffraction.* Motivated by the observed single-component adsorption behavior, we then investigated the atomic-scale source of the apparent inverted adsorption affinity for ethane over ethylene and propane over propylene in CdIF-13. To this end, we conducted *in situ* gas-dosed powder synchrotron X-ray diffraction (PSXRD) measurements at 298 K and pressures up to 20 bar with ethane, ethylene, propane, and propylene gases (Figure 2C–F) at beamline 17-BM, the Advanced Photon Source, Argonne National Laboratory. For each gas, we collected patterns at gas-dosing pressures corresponding to the prestep and poststep regimes of the isothermal adsorption data. The patterns are plotted in Figure 2 offset in the *y*-axis direction based on the *in situ* gas-dosing pressure at which they were collected. The patterns are color-coded according to the observed phases. The Bragg peaks in the blue patterns are indexed using the $P\bar{1}$ model determined from single crystal diffraction measurements.⁴⁸ As pressure increases for all four probe gases through the adsorption threshold pressure determined from the isotherm plots, the Bragg peaks arising from the dense $P\bar{1}$ phase decrease smoothly and monotonically in intensity, while new Bragg peaks appear in the pattern and increase smoothly in intensity, indicating a structural phase transition. The new set of Bragg peaks, which grow in intensity as a function of increasing gas-dosing pressure, can be successfully indexed using a slightly modified $R\bar{3}$ structural model derived from the structure of water-solvated ZIF-7 determined by single crystal XRD measurements.⁵⁵ The purple patterns in Figure 2 contain

some phase percentage of both the $P\bar{1}$ and $R\bar{3}$ phases whereas, the red patterns contain effectively just the $R\bar{3}$ phase. We observe good agreement for the pressure–temperature conditions of the phase transition for all four probe gases between the macroscopic probe of gas adsorption measurements and the microscopic probe of diffraction measurements.

Pawley fits of the PSXRD patterns yielded the lattice parameters for the two phases as a function of gas-dosing pressure (Figures S1 and S2). Notably, for all four probe gases, the lattice parameters decrease significantly between the activated structure and the first dosing concentration but then remain relatively flat as pressure increases. The flat nature of the lattice parameters suggests minimal adsorption in the dense phase, which is in agreement with the isothermal gas adsorption measurements. Above the phase change pressure, the lattice parameters for the open phase (Figure S2) are relatively flat again for ethylene, propane, and propylene, but sloped for ethane. The sloped nature of the unit cell volume suggests continued sorption as a function of increasing pressure, again in agreement with the isothermal adsorption data.

Rietveld refinements were then conducted to determine the crystal structures of gas-dosed CdIF-13 (see Supporting Information).⁵⁶ Specifically, individual Rietveld refinements were conducted for the patterns obtained at the highest measured pressure in the prestep regime of the isotherm plots for ethane, ethylene, propane, and propylene. For all four probe gases, we find that the crystal structure of the gas-dosed material in the dense phase is directly analogous to the structure of the activated material. Satisfactory Rietveld refinements consistent with the powder patterns were achieved without including gas molecules in the structural models (Figures S3–S7). Analysis of the Fourier difference maps does not indicate missing scattering density in the models. No uptake is detected by either adsorption measurements or diffraction measurements in the prestep regime, highlighting the low accessible porosity of the dense phase.

To elucidate the structure of CdIF-13 in the open phase, Rietveld refinements were then attempted for the patterns obtained at the highest measured pressure for ethane, ethylene, propane, and propylene. Satisfactory refinements that are consistent with the powder patterns yielded the crystal structures of the gas-dosed material (Figure S8–S11). The resulting crystal structures show that gas molecules adsorb at three distinct crystallographic sites, which are similar for all four gases. Analysis of the Fourier difference maps indicates that the primary adsorption site, site I, occurs in the most symmetric six-membered ring for all four gases (denoted by the blue hexagons in Figures 1B and 3). Site II occurs in the less-symmetric six-membered ring in the open phase of the material (denoted by the red hexagons in Figures 1B and 3). The third adsorption site, site III, occurs along the crystallographic *c*-axis (Figure 3, left column, Figure S12) relative to site I.

A detailed analysis of the adsorption motifs for the four probe gases helps explain the observations from the isothermal gas adsorption measurements and elucidates the mechanism enabling implied inverse selectivity in CdIF-13 (Figure 3). Subtle, key differences in adsorption site orientation between the alkene and alkane gases lead to drastically different macroscopic adsorption properties. For the C3 gases, at site I, the propane molecule is large enough to bridge the entire six-membered ring and forms four C–H $\cdots\pi$ interactions with the

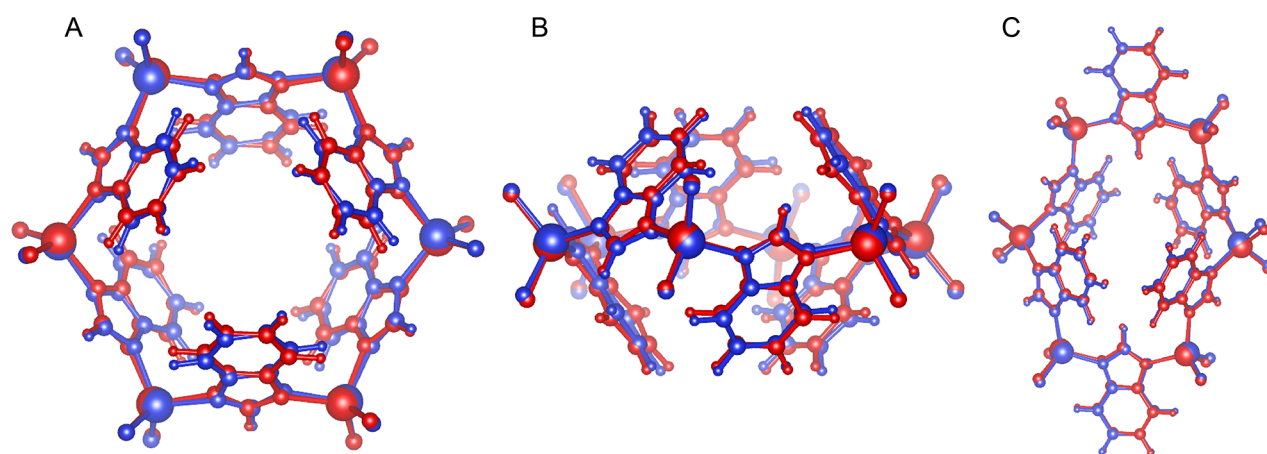


Figure 4. Subtle shifts between the propane saturated (blue) and propylene saturated (red) crystal structures at site I lead to a large change in sorption properties for the primary (A, B) and secondary (C) sorption sites.

benzimidazolate linkers ranging in length between 2.34(4) and 3.12(5) Å. These distances are consistent with moderately strong adsorption interactions.^{42,57} In contrast, the propylene molecule does not bridge the six-membered ring, and the gas molecule forms only two C–H $\cdots\pi$ interactions, which are 3.00(7) and 3.11(6) Å in length. The longer distances here suggest weaker C–H $\cdots\pi$ interactions for the olefin than for the paraffin gas. Similarly, site I for the C2 gases occurs in the most symmetric 6-membered ring. Neither gas is large enough to span the entire ring, yet the alkane molecule still forms more and closer C–H $\cdots\pi$ interactions with the benzimidazolate linkers than does the olefin gas. Ethane forms 8 distinct C–H $\cdots\pi$ interactions ranging in length from 2.22(3) to 3.11(2) Å whereas ethylene forms four such interactions, which range from 2.41(5) to 3.06(5) Å.

Similarly, at site II, propane forms more and closer C–H $\cdots\pi$ interactions with the framework than does propylene. Propane forms five C–H $\cdots\pi$ interactions between 2.78(6) and 3.19(7) Å in length, whereas propylene forms just one at 2.62(8) Å. Ethane and ethylene both form only one C–H $\cdots\pi$ interaction with the framework at site II, at distances of 3.36(2) and 3.16(2) Å, respectively.

Adsorption at site III occurs between 6 linkers, and the gas molecules form weak van der Waals interactions with the H atoms along the benzene backbone of these linkers. The number and strength of van der Waals interactions at site III are similar for propane compared with propylene and for ethane compared with ethylene. Interestingly, we observe adsorption with the molecules oriented with the *c*-axis for ethylene, propane, and propylene, but perpendicular to the crystallographic *c*-axis for ethane (Figure 3, left column, center of the skeletons). The previous study, which investigated C2 gas adsorption in ZIF-7 using density functional theory (DFT) calculations, indeed predicted differing sorption motifs between ethane and ethylene at this adsorption site.⁴³ However, this study also predicted a rearrangement of the framework between the two, which we did not observe experimentally. Also, this study did not consider sorption at site II and predicted significantly different orientations for the C2 gases at site I compared to our experimentally derived crystal structures presented herein. The structural evidence presented for CdIF-13 should be considered when explaining the inverse selectivity in isostructural ZIF-7.

Based on this detailed analysis of the individual adsorption motifs for ethane, ethylene, propane, and propylene at sites I and II, we posit that the respective ensembles of C–H $\cdots\pi$ interactions in the spontaneously tailored pore environments appear responsible for the enthalpies of adsorption for the olefin and paraffin gases. Despite the presence of π and π^* orbitals on the alkene species, the sum of the C–H $\cdots\pi$ interactions results in stronger adsorption for the alkanes than for the corresponding alkenes at the primary and secondary adsorption sites. Importantly, the absence of a strongly Lewis acidic site, such as a coordinatively unsaturated metal center, prevents strong adsorption through the π -electrons of the alkenes. Here, we provide the first detailed structural evidence for this mechanism and show that it can be generalized for the C2 and C3 gases.

First-Principles Calculations. To further understand the atomic-level surface interactions enabling inverse selectivity, we conducted first-principles dispersion-corrected DFT calculations for propane- and propylene-dosed CdIF-13. The adsorption motifs for propane and propylene found in the optimized calculated structures agree very well with the adsorption motifs determined from the Rietveld refinements of the PSXRD patterns. Based on these calculations, we find net overall enthalpies of adsorption of 34.6 and 28.5 kJ mol⁻¹ for propane and propylene, respectively (discussed in the Supporting Information section), corresponding to an $\approx 20\%$ higher affinity for propane than for propylene. This agrees with enthalpies determined from variable-temperature single-component adsorption measurements in the center of the isotherm step, which are 31.9(1) and 26.6(1) kJ mol⁻¹ for propane and propylene, respectively (Figure S13). Thus, the first-principles calculations are consistent with the experimental adsorption and diffraction experiments and corroborate the hypothesis that the adsorption sites determined from the PSXRD experiments correlate with the inverse selectivity suggested by the isothermal measurements.

Examining Adaption of the Pore Environments. We hypothesized that the phase change in CdIF-13 is cooperative, occurring across the entire crystallite in a discontinuous first-order phase transition. This contrasts with frameworks that undergo local structural perturbations in response to adsorbates and do not exhibit anomalous isothermal adsorption behavior.⁵⁸ The adsorption of the gas molecules helps template the structure of the open phase of CdIF-13,

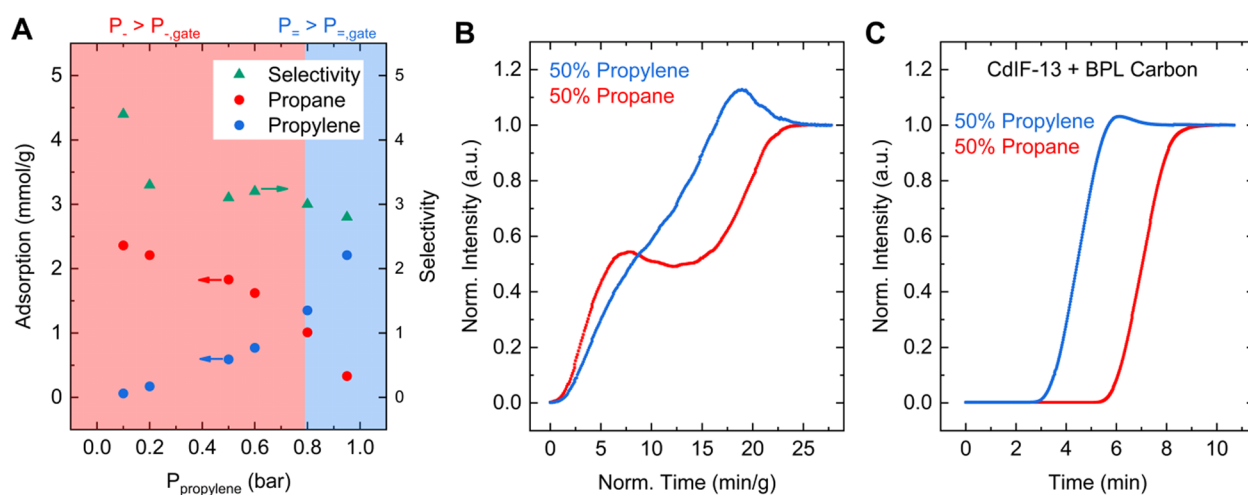


Figure 5. (A) Experimentally determined uptakes of coadsorbing propane and propylene from mixtures with varied compositions and the resulting selectivity values for propane over propylene. The gas species driving the gate opening transition is indicated by the red (propane) and blue (propylene) highlights. $P_{>}$ = propane, $P_{=}$ = propylene. Arrows point to respective axes for the colored data points. (B) Experimental fixed-bed column breakthrough curve using CdIF-13 for a propylene/propane (50:50) mixture. (C) Experimental fixed-bed column breakthrough curve for a propylene/propane (50:50) mixture on a sequential column of CdIF-13 and BPL Carbon at a carrier-free total pressure of 1.0 bar at 298 K leading to a sharp and clean separation of propane from propylene.

while at the same time, the structure of the framework dictates the location of the adsorption sites. The degree to which the structure would conform to fit the adsorbate, we hypothesized, would depend on the nature of the adsorbate. To test this hypothesis, we overlaid the structures for propane- and propylene-saturated CdIF-13. Figure 4 shows the overlay for propane-saturated (blue) and propylene-saturated (red) CdIF-13 for site I (A, B) and II (C). We observe that the degree of linker rotation is similar between the two structures for both sites. The most significant difference appears to be the degree of linker twisting relative to the plane of the Cd(II) atoms bridged by the respective linker. Indeed, these minor differences in rotations and twisting upon the adsorption of different species highlight how subtle structural changes can give rise to large changes in adsorption properties. We note that powder diffraction yields the averaged structure, and if there is local ordering that maximizes the adsorbate–adsorbent interaction, then it cannot be resolved using powder diffraction measurements.

Structural Origins of Differences in Uptake Capacities. Next, we analyzed the powder data to better understand the remaining observations from the isothermal adsorption measurements—the overall increase in adsorption for the C2 vs C3 gases and the sloped nature of the poststep regime of the isothermal plot for ethane. The overall increased adsorption observed in the isothermal measurements for the C2 gases compared to the C3 gases can be understood at the atomic scale based on the crystal structures of gas-dosed CdIF-13. Adsorption at sites I, II, and III is disordered for the C2 and C3 gases. For the larger C3 gases, only one molecule can adsorb at the three different sites (once positional disorder is accounted for). However, for the smaller C2 gases, two molecules can simultaneously adsorb at sites I and II, leading to gas–gas interactions that stabilize the sorption sites in energy. The increased overall adsorption for the C2 gases compared to the C3 gases observed in the adsorption measurements can be understood based on the more efficient packing of the smaller molecules. Again, the amount of gas determined from the Rietveld refinements at each condition

agrees well with the amount of gas adsorbed as determined by the isothermal measurements (Table S6).

In addition, the sloped nature of ethane adsorption in the poststep regime can be better understood at an atomic scale by examining the ethane occupancies at sites I and II as a function of pressure (Table S6). At intermediate pressures, only one equivalent of gas crystallizes at these sites. With an increase in pressure, a second equivalent of gas crystallizes at both sites. The interplay between steric effects at each site, the applied external pressure, and, likely, the kinetics of gas diffusion determines the number of gas molecules and thus the overall amount of gas adsorbed over the time scale of the experiment.

Macroscale Effects on Phase Change Conditions. Finally, we attempted to rationalize the coexistence of the dense and open phases at intermediate pressures observed in the PSXRD patterns plotted in purple in Figure 2C–F. In the prestep regime of the isothermal adsorption plots, the amount of gas is nearly zero for all probe gases measured here, as determined by the isotherm adsorption measurements, and no gas is detected in the bulk of the material by the Rietveld refinements of the PSXRD patterns. This indicates effective pore gating of the interior of the particles comprising the powder samples. It is hypothesized that initial adsorption events occur at the surface of the individual crystallite particles, with the adsorbed gas inducing a strain field in the particle. A critical amount of adsorption-induced strain in the particles induces the phase transition. The pressure at which this critical strain occurs is related to the enthalpy of adsorption, with more strongly interacting species inducing critical strain at lower pressures. This critical amount of adsorption-induced strain may be determined by particle properties such as particle size,^{59–64} particle morphology,^{65,66} local defects, local pressure gradients, and/or crystallite strain.^{67,68} Similar behavior has been hypothesized for $Zn_2(\text{bdc})_2(\text{bpy})_n$ (bdc = 1,4-benzenedicarboxylate, bpy = 4,4'-bipyridine).⁶⁷ Here, we hypothesize that the transition is first order on a per-particle basis and that a distribution of particle properties in the powder sample leads to the observation of both phases simultaneously in the PSXRD data.

Propane/Propylene Dynamic Breakthrough Experiments. At the core of this effort, we sought to both understand how cooperatively flexible materials can maintain selectivity under dynamic mixed-gas conditions and advance the ability to directly purify propylene by removing the minor component propane under ambient conditions. Therefore, to quantify and confirm the persistence of the inverse selectivity toward propane over propylene in CdIF-13 under direct mixture conditions, we then performed binary dynamic column breakthrough experiments at a carrier-free pressure of 1 bar at 298 K using a pelletized, crushed, and sieved sample over a representatively broad range of propane/propylene mixture compositions. We note that the high pressures of ethane/ethylene adsorption precluded similar measurements for C2 species. Control adsorption measurements validate the maintained performance of the pelletized CdIF-13 (Figure S14, Supporting Information). In the breakthrough measurements, the combined pressure of the adsorbing species was held constant at 1 bar such that, for any one measurement, the partial pressure of either propane or propylene exceeded their respective step pressure thresholds determined by the single-component isothermal adsorption measurements (Figure 2A, highlighted regions in Figure 5A). Quite excitingly, these measurements (Figure S15, Supporting Information discussion) indicate that everywhere between 10:90 and 95:5 propylene/propane ratios, CdIF-13 competitively adsorbs propane, even when the partial pressure of propane is below its respective step pressure threshold (Figure 5A). Between 10 and 20% propylene content, the separation factor ($\alpha = \frac{q(\text{propylene})}{q(\text{propane})} \cdot \frac{p(\text{propane})}{p(\text{propylene})}$) (q = quantity adsorbed, p = partial pressure) reduces from ≈ 4.4 to ≈ 3.3 , remains constant at ≈ 3.1 between 20 and 80% propylene, and remains ≈ 2.8 at even 95% propylene.

Though the selectivity of 3.1 for a 50:50 mixture is a modest 15% increase compared to ZIF-7 at 1 bar and 298 K,⁴³ separation factors at higher ratios are more relevant as propylene production via cracking processes produces an extreme propylene-rich, propane-poor mixture, typically between 93–95% propylene (7–5% propane).²¹ Critically, separation factors for previously reported materials tend to deteriorate under propylene-rich conditions. For the best-performing materials, this can be experimentally confirmed with breakthrough measurements. For example, in the metal–organic frameworks PCP-IPA, the best-performing material in the literature to date, the separation factor decreases from 2.09 at an equimolar mixture ratio to 2.06 at 95:5 propylene:propane ratios.⁶⁹ More significantly, ZIF-67,²⁷ ZIF-8,²³ and ZIF-4,²⁴ exhibit separation factors of only 1.35, 1.25, and 1.06, respectively, where $P_{\text{propylene}} \geq 0.80$ bar (Tables S1 and S10). In stark contrast, the high separation factor exhibited by CdIF-13 persists at 95:5 propylene/propane, representative of industrial mixtures. In addition, CdIF-13 shows a higher amount of adsorbed propane (0.33 mmol g⁻¹) compared to PCP-IPA (0.24 mmol g⁻¹) at this condition (Table S10).⁶⁹ Moreover, this is achieved at ambient temperature and pressure. Thus, cooperatively flexible CdIF-13 displays the highest ever reported experimentally derived separation factor under conditions of 80% propylene and above, even at industrially relevant 95:5 mixture conditions, suggesting that propylene could be directly purified at 298 K and 1 bar.

Accordingly, we sought to optimize the propylene purification process to determine whether this material could be integrated with industrial column-based separation technologies. We noted that the breakthrough curve for a 50:50 mixture of 1 bar propylene/propane displays a slipping-off effect (Figure 5B, Supporting Information discussion).⁵² This slipping-off effect persists for both components until the propane partial pressure builds to exceed the adsorption pressure threshold determined by single-component equilibrium adsorption measurements (Figures 2A,B and S16). When the pressure threshold is met, the open framework structure preferentially adsorbs propane while propylene breaks through. Due to the higher enthalpy of adsorption of propane, it displaces the more weakly adsorbing propylene in the CdIF-13 column and causes an effect known as roll-up,^{70,71} as seen in Figure 5B, where propylene exceeds its inlet concentration above 1.0 (Supporting Information discussion). To eliminate the initial slipping-off effect, we employed a sequential column approach.⁵² We sought an inexpensive and abundant material with typical selectivity for propylene to leverage the desired inverse selectivity stemming from CdIF-13, eliminate slip-off, and immediately produce purified propylene downstream. Indeed, when we utilized the activated carbon BPL Carbon in the second column, the slipping-off phenomenon was not observed and a sharp, clean separation was realized, producing purified propylene in a flow-based process at room temperature and 1 bar (Figure 5C and Supporting Information). The size-optimized BPL Carbon bed captures the mixture flown through the CdIF-13 bed while the latter undergoes the phase transition, without contributing to the separation, and is saturated exactly when the separation in the open structure of CdIF-13 takes place (Supporting Information discussion and Figure S53). A proposed process integration to readily cycle this two-column system is described in the Supporting Information discussion (Figures S17 and S53) but requires experimental validation in future work. We acknowledge that the record-high separation factors achieved here in a two-column approach may not be directly comparable to separation factors achieved in a single-column approach. However, we posit that the comparison to other materials in the literature (Table S1) is still important, warranted, and valid given that the role of the BPL carbon here is to mitigate slipping-off and roll-up effects (Figure S53), and that the self-adjusting flexibility of CdIF-13 to form optimized adsorption pockets for each gas drives the separation. To probe cyclability, we conducted additional single-component propane isothermal adsorption measurements, which illustrate that the phase transition is robust, reproducible, and cycleable up to 15 cycles (Figure S54). We also conducted cycled single-column breakthrough measurements (Figure S55) which illustrate that the results are highly consistent over several cycles. Moreover, the roll-up effect is mitigated after the first cycle for a single column experiment, likely due to interparticle effects from pelletization seen in the first cycle and mitigated after the completion of a phase transition-regeneration cycle.

CONCLUSIONS

In summary, we showed that the cooperatively flexible metal–organic framework CdIF-13 (*sod*-Cd-(benzimidazolates)₂) exhibits record separation factors over a large range of propane/propylene mixture concentrations, including at industrially relevant propylene-rich ratios. In situ gas-dosed PSXRD measurements coupled with first-principles

calculations reveal the atomic-level origins of the observed separation capabilities. Namely, the framework spontaneously adapts its pore structure to a given adsorbate to form an ensemble of individually weak surface interactions that lead to thermodynamic preferences for the adsorption of C2 and C3 alkanes over alkenes. This detailed structure–function relationship helps shed light on how cooperatively flexible framework materials adsorb different gases and provides the first experimental evidence corroborating and updating a hypothesis in the literature explaining inverse selectivity in ZIF-7 since the seminal work on this material was published more than a decade ago. To take our study one step further, direct propylene purification was achieved using CdIF-13 in a double column breakthrough approach—pairing an inexpensive rigid material with a flexible material displaying inverse selectivity—obviating slipping-off and producing purified propylene downstream at ambient temperature and pressure and at industrially relevant mixture conditions. This work highlights the general principle that cooperative framework flexibility can create thermodynamically optimized adsorption environments for industrially critical feedstocks that function under dynamic mixed-component breakthrough conditions, which has broad-ranging and immediate implications for separations, storage, catalysis, and capture technologies.

■ ASSOCIATED CONTENT

SI Supporting Information

The Supporting Information is available free of charge at <https://pubs.acs.org/doi/10.1021/jacs.3c06754>.

Details of framework synthesis and characterization, low- and high-pressure gas adsorption measurements and analysis, and PSXRD measurements and analysis (PDF)

Accession Codes

CCDC 2241912–2241932 contain the supplementary crystallographic data for this paper. These data can be obtained free of charge via www.ccdc.cam.ac.uk/data_request/cif, or by emailing data_request@ccdc.cam.ac.uk, or by contacting The Cambridge Crystallographic Data Centre, 12 Union Road, Cambridge CB2 1EZ, UK; fax: +44 1223 336033.

■ AUTHOR INFORMATION

Corresponding Author

C. Michael McGuirk – Department of Chemistry, Colorado School of Mines, Golden, Colorado 80401, United States; orcid.org/0000-0002-7420-1169; Email: cmmcguirk@mines.edu

Authors

Ryan A. Klein – Materials, Chemical, and Computational Sciences, National Renewable Energy Laboratory, Golden, Colorado 80401, United States; Center for Neutron Research, National Institute of Standards and Technology, Gaithersburg, Maryland 20899, United States

Lukas W. Bingel – School of Chemical & Biomolecular Engineering, Georgia Institute of Technology, Atlanta, Georgia 30332, United States

Arijit Halder – Department of Chemistry, Colorado School of Mines, Golden, Colorado 80401, United States; orcid.org/0000-0002-4047-2593

Marcus Carter – Center for Neutron Research, National Institute of Standards and Technology, Gaithersburg, Maryland 20899, United States

Benjamin A. Trump – Center for Neutron Research, National Institute of Standards and Technology, Gaithersburg, Maryland 20899, United States

Eric D. Bloch – Department of Chemistry and Biochemistry, University of Delaware, Newark, Delaware 19716, United States; orcid.org/0000-0003-4507-6247

Wei Zhou – Center for Neutron Research, National Institute of Standards and Technology, Gaithersburg, Maryland 20899, United States; orcid.org/0000-0002-5461-3617

Krista S. Walton – School of Chemical & Biomolecular Engineering, Georgia Institute of Technology, Atlanta, Georgia 30332, United States

Craig M. Brown – Center for Neutron Research, National Institute of Standards and Technology, Gaithersburg, Maryland 20899, United States; Department of Chemical Engineering, University of Delaware, Newark, Delaware 19716, United States; orcid.org/0000-0002-9637-9355

Complete contact information is available at:

<https://pubs.acs.org/10.1021/jacs.3c06754>

Author Contributions

[▽]R.A.K. and L.W.B. contributed equally to this work.

Notes

The authors declare no competing financial interest.

■ ACKNOWLEDGMENTS

We thank Drs. Andrey Yakovenko and Wenqian Xu for their technical assistance. Certain commercial equipment, instruments, or materials are identified in this document. Such identification does not imply recommendation or endorsement by the National Institute of Standards and Technology, nor does it imply that the products identified are necessarily the best available for the purpose. The views expressed in the article do not necessarily represent the views of the DOE or the U.S. Government. The U.S. Government retains, and the publisher, by accepting the article for publication, acknowledges that the U.S. Government retains a nonexclusive, paid-up, irrevocable, worldwide license to publish or reproduce the published form of this work, or allow others to do so, for U.S. Government purposes. Powder X-ray diffraction data were collected on beamline 17-BM at the Advanced Photon Source, Argonne National Laboratory, which is supported by the U.S. Department of Energy (U.S. DOE), Office of Science, and Office of Basic Energy Sciences under Contract DEAC02-06CH11357. R.A.K. gratefully acknowledges funding from the U.S. DOE, Office of Energy Efficiency and Renewable Energy (EERE), Hydrogen and Fuel Cell Technologies Office (HFTO) contract no. DE-AC36-8GO28308 to the National Renewable Energy Laboratory (NREL). L.W.B. and K.S.W. acknowledge funding from the Georgia Institute of Technology. A.H. and C.M.M. gratefully acknowledge funding from the U.S. DOE EERE HFTO under Award Number DE-EE0008823.

■ REFERENCES

- (1) Sholl, D. S.; Lively, R. P. Seven Chemical Separations to Change the World. *Nature* **2016**, 532 (7600), 435–437.
- (2) Koros, W. J.; Lively, R. P. Water and Beyond: Expanding the Spectrum of Large-Scale Energy Efficient Separation Processes. *AIChE J.* **2012**, 58 (9), 2624.
- (3) Eldridge, R. B. Olefin/paraffin Separation Technology: A Review. *Ind. Eng. Chem. Res.* **1993**, 32 (10), 2208–2212.

- (4) Safarik, D. J.; Eldridge, R. B. Olefin/paraffin Separations by Reactive Absorption: A Review. *Ind. Eng. Chem. Res.* **1998**, *37* (7), 2571–2581.
- (5) Wang, Y.; Peh, S. B.; Zhao, D. Alternatives to Cryogenic Distillation: Advanced Porous Materials in Adsorptive Light Olefin/paraffin Separations. *Small* **2019**, *15* (25), No. 1900058.
- (6) Amghizar, I.; Vandewalle, L. A.; Van Geem, K. M.; Marin, G. B. New Trends in Olefin Production. *Engineering* **2017**, *3* (2), 171–178.
- (7) Ren, T.; Patel, M.; Blok, K. Olefins from Conventional and Heavy Feedstocks: Energy Use in Steam Cracking and Alternative Processes. *Energy* **2006**, *31* (4), 425–451.
- (8) Sircar, S.; Golden, T.; Rao, M. Activated Carbon for Gas Separation and Storage. *Carbon* **1996**, *34* (1), 1–12.
- (9) Ackley, M. W.; Rege, S. U.; Saxena, H. Application of Natural Zeolites in the Purification and Separation of Gases. *Microporous Mesoporous Mater.* **2003**, *61* (1–3), 25–42.
- (10) Zhou, H.-C.; Long, J. R.; Yaghi, O. M. Introduction to Metal–Organic Frameworks. *Chem. Rev.* **2012**, *112* (2), 673–674.
- (11) Lin, R.-B.; Xiang, S.; Xing, H.; Zhou, W.; Chen, B. Exploration of Porous Metal–Organic Frameworks for Gas Separation and Purification. *Coord. Chem. Rev.* **2019**, *378*, 87–103.
- (12) Barnett, B. R.; Gonzalez, M. I.; Long, J. R. Recent Progress Towards Light Hydrocarbon Separations Using Metal–Organic Frameworks. *Trends Chem.* **2019**, *1* (2), 159–171.
- (13) Gu, X.-W.; Wang, J.-X.; Wu, E.; Wu, H.; Zhou, W.; Qian, G.; Chen, B.; Li, B. Immobilization of Lewis Basic Sites into a Stable Ethane-Selective MOF Enabling One-Step Separation of Ethylene from a Ternary Mixture. *J. Am. Chem. Soc.* **2022**, *144* (6), 2614–2623.
- (14) Li, L.; Lin, R.-B.; Krishna, R.; Li, H.; Xiang, S.; Wu, H.; Li, J.; Zhou, W.; Chen, B. Ethane/ethylene Separation in a Metal–Organic Framework with Iron-Peroxo Sites. *Science* **2018**, *362* (6413), 443–446.
- (15) Liao, P.-Q.; Zhang, W.-X.; Zhang, J.-P.; Chen, X.-M. Efficient Purification of Ethene by an Ethane-Trapping Metal–Organic Framework. *Nat. Commun.* **2015**, *6* (1), 8697.
- (16) Lin, R.-B.; Wu, H.; Li, L.; Tang, X.-L.; Li, Z.; Gao, J.; Cui, H.; Zhou, W.; Chen, B. Boosting Ethane/ethylene Separation Within Isorecticular Ultramicroporous Metal–Organic Frameworks. *J. Am. Chem. Soc.* **2018**, *140* (40), 12940–12946.
- (17) Qazvini, O. T.; Babarao, R.; Shi, Z.-L.; Zhang, Y.-B.; Telfer, S. G. A Robust Ethane-Trapping Metal–Organic Framework with a High Capacity for Ethylene Purification. *J. Am. Chem. Soc.* **2019**, *141* (12), 5014–5020.
- (18) Zeng, H.; Xie, X.-J.; Xie, M.; Huang, Y.-L.; Luo, D.; Wang, T.; Zhao, Y.; Lu, W.; Li, D. Cage-Interconnected Metal–Organic Framework with Tailored Apertures for Efficient C₂H₆/C₂H₄ Separation Under Humid Conditions. *J. Am. Chem. Soc.* **2019**, *141* (51), 20390–20396.
- (19) Cai, X.; Gharagheizi, F.; Bingel, L. W.; Shade, D.; Walton, K. S.; Sholl, D. S. A Collection of More Than 900 Gas Mixture Adsorption Experiments in Porous Materials from Literature Meta-Analysis. *Ind. Eng. Chem. Res.* **2021**, *60* (1), 639–651.
- (20) Yang, H.; Wang, Y.; Krishna, R.; Jia, X.; Wang, Y.; Hong, A. N.; Dang, C.; Castillo, H. E.; Bu, X.; Feng, P. Pore-Space-Partition-Enabled Exceptional Ethane Uptake and Ethane-Selective Ethane–Ethylene Separation. *J. Am. Chem. Soc.* **2020**, *142* (5), 2222–2227.
- (21) Van Willigengburg. C3 Fractionation System. Pat. No.: US 11,174,209 B2. 2021.
- (22) Bendt, S.; Hovestadt, M.; Böhme, U.; Paula, C.; Döpken, M.; Hartmann, M.; Keil, F. J. Olefin/Paraffin Separation Potential of ZIF-9 and ZIF-71: A Combined Experimental and Theoretical Study. *Eur. J. Inorg. Chem.* **2016**, *2016* (27), 4440–4449.
- (23) Böhme, U.; Barth, B.; Paula, C.; Kuhnt, A.; Schwieger, W.; Mundstock, A.; Caro, J.; Hartmann, M. Ethene/Ethane and Propene/Propane Separation via the Olefin and Paraffin Selective Metal–Organic Framework Adsorbents CPO-27 and ZIF-8. *Langmuir* **2013**, *29* (27), 8592–8600.
- (24) Hartmann, M.; Böhme, U.; Hovestadt, M.; Paula, C. Adsorptive Separation of Olefin/Paraffin Mixtures with ZIF-4. *Langmuir* **2015**, *31* (45), 12382–12389.
- (25) Lewis, W. K.; Gilliland, E. R.; Chertow, B.; Hoffman, W. H. Vapor–Adsorbate¹ Equilibrium. I. Propane–Propylene on Activated Carbon and on Silica Gel. *J. Am. Chem. Soc.* **1950**, *72* (3), 1153–1157.
- (26) Glanz, P.; Findenegg, G. Adsorption of Gas Mixtures of Propene and Propane on Graphitized Carbon Black I. Experimental Method and Results. *Adsorpt. Sci. Technol.* **1984**, *1* (1), 41–50.
- (27) Andres-Garcia, E.; Oar-Arteta, L.; Gascon, J.; Kapteijn, F. ZIF-67 as Silver-Bullet in Adsorptive Propane/propylene Separation. *Chem. Eng. J.* **2019**, *360*, 10–14.
- (28) Andres-Garcia, E.; López-Cabrelles, J.; Oar-Arteta, L.; Roldan-Martinez, B.; Cano-Padilla, M.; Gascon, J.; Espallargas, G. M.; Kapteijn, F. Cation Influence in Adsorptive Propane/propylene Separation in ZIF-8 (SOD) Topology. *Chem. Eng. J.* **2019**, *371*, 848–856.
- (29) Yang, L.; Cui, X.; Ding, Q.; Wang, Q.; Jin, A.; Ge, L.; Xing, H. Polycatenated Molecular Cage-Based Propane Trap for Propylene Purification with Recorded Selectivity. *ACS Appl. Mater. Interfaces* **2020**, *12* (2), 2525–2530.
- (30) Chang, M.; Ren, J.; Wei, Y.; Wang, J.-X.; Yang, Q.; Liu, D.; Chen, J.-F. A Robust Metal–Organic Framework with Guest Molecules Induced Splint-Like Pore Confinement to Construct Propane-Trap for Propylene Purification. *Sep. Purif. Technol.* **2021**, *279*, No. 119656.
- (31) Yang, S.-Q.; Sun, F.-Z.; Krishna, R.; Zhang, Q.; Zhou, L.; Zhang, Y.-H.; Hu, T.-L. Propane-Trapping Ultramicroporous Metal–Organic Framework in the Low-Pressure Area Toward the Purification of Propylene. *ACS Appl. Mater. Interfaces* **2021**, *13* (30), 35990–35996.
- (32) He, C.; Wang, Y.; Chen, Y.; Wang, X.; Yang, J.; Li, L.; Li, J. Modification of the Pore Environment in UiO-Type Metal–Organic Framework Toward Boosting the Separation of Propane/propylene. *Chem. Eng. J.* **2021**, *403*, No. 126428.
- (33) Hong, A. N.; Yang, H.; Li, T.; Wang, Y.; Wang, Y.; Jia, X.; Zhou, A.; Kusumoputro, E.; Li, J.; Bu, X.; Feng, P. Pore-Space Partition and Optimization for Propane-Selective High-Performance Propane/Propylene Separation. *ACS Appl. Mater. Interfaces* **2021**, *13* (44), 52160–52166.
- (34) Van Den Bergh, J.; Gücüyener, C.; Pidko, E. A.; Hensen, E. J.; Gascon, J.; Kapteijn, F. Understanding the Anomalous Alkane Selectivity of ZIF-7 in the Separation of Light Alkane/alkene Mixtures. *Chem.–Eur. J.* **2011**, *17* (32), 8832–8840.
- (35) Wang, S.; Zhang, Y.; Tang, Y.; Wen, Y.; Lv, Z.; Liu, S.; Li, X.; Zhou, X. Propane-Selective Design of Zirconium-Based MOFs for Propylene Purification. *Chem. Eng. Sci.* **2020**, *219*, No. 115604.
- (36) Iacomì, P.; Formalik, F.; Marreiros, J.; Shang, J.; Rogacka, J.; Mohmeyer, A.; Behrens, P.; Ameloot, R.; Kuchta, B.; Llewellyn, P. L. Role of Structural Defects in the Adsorption and Separation of C3 Hydrocarbons in Zr-Fumarate-MOF (MOF-801). *Chem. Mater.* **2019**, *31* (20), 8413–8423.
- (37) Li, X.; Liu, J.; Zhou, K.; Ullah, S.; Wang, H.; Zou, J.; Thonhauser, T.; Li, J. Tuning Metal–Organic Framework (MOF) Topology by Regulating Ligand and Secondary Building Unit (SBU) Geometry: Structures Built on 8-Connected M₆ (M = Zr, Y) Clusters and a Flexible Tetracarboxylate for Propane-Selective Propane/Propylene Separation. *J. Am. Chem. Soc.* **2022**, *144* (47), 21702–21709.
- (38) Sholl, D. S.; Lively, R. P. Exemplar Mixtures for Studying Complex Mixture Effects in Practical Chemical Separations. *JACS Au* **2022**, *2* (2), 322–327.
- (39) Yang, L.; Qian, S.; Wang, X.; Cui, X.; Chen, B.; Xing, H. Energy-Efficient Separation Alternatives: Metal–Organic Frameworks and Membranes for Hydrocarbon Separation. *Chem. Soc. Rev.* **2020**, *49* (15), 5359–5406.
- (40) Trump, B. A.; Qazvini, O. T.; Lee, S. J.; Jangodaz, E.; Zhou, W.; Brown, C. M.; Telfer, S. G. Flexing of a Metal–Organic Framework

Upon Hydrocarbon Adsorption: Atomic Level Insights from Neutron Scattering. *Chem. Mater.* **2023**, *35* (3), 1387–1394.

(41) Bereciartua, P. J.; Cantin, A.; Corma, A.; Jordá, J. L.; Palomino, M.; Rey, F.; Valencia, S.; Corcoran, E. W., Jr; Kortunov, P.; Ravikovitch, P. I.; others. Control of Zeolite Framework Flexibility and Pore Topology for Separation of Ethane and Ethylene. *Science* **2017**, *358* (6366), 1068–1071.

(42) Halter, D. P.; Klein, R. A.; Boreen, M. A.; Trump, B. A.; Brown, C. M.; Long, J. R. Self-Adjusting Binding Pockets Enhance H₂ and CH₄ Adsorption in a Uranium-Based Metal–Organic Framework. *Chem. Sci.* **2020**, *11* (26), 6709–6716.

(43) Gücüyener, C.; van den Bergh, J.; Gascon, J.; Kapteijn, F. Ethane/Ethene Separation Turned on Its Head: Selective Ethane Adsorption on the Metal–Organic Framework ZIF-7 Through a Gate-Opening Mechanism. *J. Am. Chem. Soc.* **2010**, *132* (50), 17704–17706.

(44) Xiao, Y.; Chen, Y.; Wang, W.; Yang, H.; Hong, A. N.; Bu, X.; Feng, P. Simultaneous Control of Flexibility and Rigidity in Pore-Space-Partitioned Metal–Organic Frameworks. *J. Am. Chem. Soc.* **2023**, *145* (20), 10980–10986.

(45) Jin, H.; Li, Y. Flexibility of Metal–Organic Frameworks for Separations: Utilization, Suppression and Regulation. *Curr. Opin. Chem. Eng.* **2018**, *20*, 107–113.

(46) Taylor, M. K.; Runčevski, T.; Oktawiec, J.; Bachman, J. E.; Siegelman, R. L.; Jiang, H.; Mason, J. A.; Tarver, J. D.; Long, J. R. Near-Perfect CO₂/CH₄ Selectivity Achieved Through Reversible Guest Templating in the Flexible Metal–Organic Framework Co(bdp). *J. Am. Chem. Soc.* **2018**, *140* (32), 10324–10331.

(47) Kauffman, K. L.; Culp, J. T.; Allen, A. J.; Espinal, L.; Wong-Ng, W.; Brown, T. D.; Goodman, A.; Bernardo, M. P.; Pancoast, R. J.; Chirdon, D.; Matranga, C. Selective Adsorption of CO₂ from Light Gas Mixtures by Using a Structurally Dynamic Porous Coordination Polymer. *Angew. Chem., Int. Ed.* **2011**, *50* (46), 10888–10892.

(48) Klein, R. A.; Shulda, S.; Parilla, P. A.; Le Magueres, P.; Richardson, R. K.; Morris, W.; Brown, C. M.; McGuirk, C. M. Structural Resolution and Mechanistic Insight into Hydrogen Adsorption in Flexible ZIF-7. *Chem. Sci.* **2021**, *12* (47), 15620–15631.

(49) Halder, A.; Klein, R. A.; Lively, R.; McGuirk, C. M. Multivariate Zeolitic Imidazolate Frameworks with an Inverting Trend in Flexibility. *Chem. Commun.* **2022**, *58* (81), 11394–11397.

(50) Halder, A.; Klein, R. A.; Shulda, S.; McCarver, G. A.; Parilla, P. A.; Furukawa, H.; Brown, C. M.; McGuirk, C. M. Multivariate Flexible Framework with High Usable Hydrogen Capacity in a Reduced Pressure Swing Process. *J. Am. Chem. Soc.* **2023**, *145* (14), 8033–8042.

(51) Boyd, P. G.; Chidambaram, A.; García-Díez, E.; Ireland, C. P.; Daff, T. D.; Bounds, R.; Gladysiak, A.; Schouwink, P.; Moosavi, S. M.; Maroto-Valer, M. M. Data-Driven Design of Metal–Organic Frameworks for Wet Flue Gas CO₂ Capture. *Nature* **2019**, *576* (7786), 253–256.

(52) Hiraide, S.; Sakanaka, Y.; Kajiro, H.; Kawaguchi, S.; Miyahara, M. T.; Tanaka, H. High-Throughput Gas Separation by Flexible Metal–Organic Frameworks with Fast Gating and Thermal Management Capabilities. *Nat. Commun.* **2020**, *11* (1), 3867.

(53) Rouquerol, J.; Rouquerol, F.; Llewellyn, P.; Maurin, G.; Sing, K. S. W. *Adsorption by powders and porous solids: principles, methodology and applications*, 2nd edition; Academic Press, 2013.

(54) McGuirk, C. M.; Runčevski, T.; Oktawiec, J.; Turkiewicz, A.; Taylor, M. K.; Long, J. R. Influence of Metal Substitution on the Pressure-Induced Phase Change in Flexible Zeolitic Imidazolate Frameworks. *J. Am. Chem. Soc.* **2018**, *140* (46), 15924–15933.

(55) Park, K. S.; Ni, Z.; Côté, A. P.; Choi, J. Y.; Huang, R.; Uribe-Romo, F. J.; Chae, H. K.; O’Keeffe, M.; Yaghi, O. M. Exceptional Chemical and Thermal Stability of Zeolitic Imidazolate Frameworks. *Proc. Natl. Acad. Sci. U. S. A.* **2006**, *103* (27), 10186–10191.

(56) Rietveld, H. M. A Profile Refinement Method for Nuclear and Magnetic Structures. *J. Appl. Crystallogr.* **1969**, *2* (2), 65–71.

(57) Hulvey, Z.; Vlaisavljevich, B.; Mason, J. A.; Tsivion, E.; Dougherty, T. P.; Bloch, E. D.; Head-Gordon, M.; Smit, B.; Long, J. R.; Brown, C. M. Critical Factors Driving the High Volumetric Uptake of Methane in Cu₃(btc)₂. *J. Am. Chem. Soc.* **2015**, *137* (33), 10816–10825.

(58) Zhou, D.-D.; Zhang, J.-P. On the Role of Flexibility for Adsorptive Separation. *Acc. Chem. Res.* **2022**, *55* (20), 2966–2977.

(59) Krause, S.; Bon, V.; Senkovska, I.; Töbrens, D. M.; Wallacher, D.; Pillai, R. S.; Maurin, G.; Kaskel, S. The effect of crystallite size on pressure amplification in switchable porous solids. *Nat. Commun.* **2018**, *9*, 1573.

(60) Zhang, C.; Gee, J. A.; Sholl, D. S.; Lively, R. P. Crystal-size-dependent structural transitions in nanoporous crystals: adsorption-induced transitions in ZIF-8. *J. Phys. Chem. C* **2014**, *118*, 20727–20733.

(61) Linder-Patton, O. M.; Bloch, W. M.; Coghlan, C. J.; Sumida, K.; Kitagawa, S.; Furukawa, S.; Doonan, C. J.; Sumbly, C. J. Particle size effects in the kinetic trapping of a structurally-locked form of a flexible MOF. *CrystEngComm* **2016**, *18*, 4172–4179.

(62) Hijikata, Y.; Horike, S.; Tanaka, D.; Groll, J.; Mizuno, M.; Kim, J.; Takata, M.; Kitagawa, S. Differences of crystal structure and dynamics between a soft porous nanocrystal and a bulk crystal. *Chem. Commun.* **2011**, *47*, 7632–7634.

(63) Kundu, T.; Wahiduzzaman, M.; Shah, B. B.; Maurin, G.; Zhao, D. Solvent-induced control over breathing behavior in flexible metal–organic frameworks for natural-gas delivery. *Angew. Chem., Int. Ed.* **2019**, *131*, 8157–8161.

(64) Zhang, J.-P.; Zhou, H.-L.; Zhou, D.-D.; Liao, P.-Q.; Chen, X.-M. Controlling flexibility of metal–organic frameworks. *Natl. Sci. Rev.* **2018**, *5*, 907–919.

(65) Shivanna, M.; Yang, Q.-Y.; Bajpai, A.; Patyk-Kazmierczak, E.; Zaworotko, M. J. A dynamic and multi-responsive porous flexible metal–organic material. *Nat. Commun.* **2018**, *9*, 3080.

(66) Linder-Patton, O. M.; Rogers, B. T.; Sumida, K. Impact of Higher-Order Structuralization on the Adsorptive Properties of Metal–Organic Frameworks. *Chem.—Asian J.* **2018**, *13*, 1979–1991.

(67) Sakata, Y.; Furukawa, S.; Kondo, M.; Hirai, K.; Horike, N.; Takashima, Y.; Uehara, H.; Louvain, N.; Meilikhov, M.; Tsuruoka, T.; Isoda, S.; Kosaka, W.; Sakata, O.; Kitagawa, S. Shape-Memory Nanopores Induced in Coordination Frameworks by Crystal Downsizing. *Science* **2013**, *339*, 193.

(68) Liu, Y.; Her, J.-H.; Dailly, A.; Ramirez-Cuesta, A. J.; Neumann, D. A.; Brown, C. M. Reversible structural transition in MIL-53 with large temperature hysteresis. *J. Am. Chem. Soc.* **2008**, *130*, 11813–11818.

(69) Zhang, P.; Yang, L.; Liu, X.; Wang, J.; Suo, X.; Chen, L.; Cui, X.; Xing, H. Ultramicroporous Material Based Parallel and Extended Paraffin Nano-Trap for Benchmark Olefin Purification. *Nat. Commun.* **2022**, *13* (1), 4928.

(70) Kapoor, A.; Yang, R. Roll-up in Fixed-Bed, Multicomponent Adsorption Under Pore-Diffusion Limitation. *AIChE J.* **1987**, *33* (7), 1215–1217.

(71) Li, G.; Xiao, P.; Xu, D.; Webley, P. A. Dual Mode Roll-up Effect in Multicomponent Non-Isothermal Adsorption Processes with Multilayered Bed Packing. *Chem. Eng. Sci.* **2011**, *66* (9), 1825–1834.